Molecular Catalysis 518 (2022) 112095

Contents lists available at ScienceDirect

Molecular Catalysis

journal homepage: www.journals.elsevier.com/molecular-catalysis

Enhancing catalytic properties of ligand-protected gold-based 25-metal atom nanoclusters by silver doping

Ricca Rahman Nasaruddin [a,b,*], Max J. Hülsey [a], Jianping Xie [a,*]

[a] Department of Chemical and Biomolecular Engineering, National University of Singapore, 4 Engineering Drive 4, 117585 Singapore
[b] Department of Biotechnology Engineering, Kulliyyah of Engineering, International Islamic University Malaysia, Jalan Gombak, Kuala Lumpur 53100, Malaysia

ARTICLE INFO

Keywords:
Bimetallic nanoclusters
Gold nanoclusters
Gold-silver nanoclusters
4-nitrophenol hydrogenation

ABSTRACT

Herein, engineering metal composition of metal nanoclusters (NCs) by foreign metal doping was used as an approach to synthesize gold (Au)-based 25-metal NC catalysts, without compromising the presence of their ligands and unique structure of 25 metal atoms. The Au-based 25-metal atom NCs with silver doping which can also be called as bimetallic AuAg NCs (*i.e.,* $Au_{25-x}Ag_x(SR)_{18}$ NCs with $x = 4–12$) were successfully synthesized by co-reduction method with various feeding ratios ($R_{Au/Ag}$ = 24/1, 22/3 and 18/7). The Ag dopants favorably replaced Au(0) atom on the vertex of the icosahedral core and enhanced the catalytic activity of bimetallic $Au_{25-x}Ag_x(SR)_{18}$ NCs due to combination of several factors. As compared to monometallic $Au_{25}(SR)_{18}$ NCs, $Au_{25-x}Ag_x(SR)_{18}$ NCs have (1) synergistic effects of Au and Ag atoms; (2) better ligands removal's and active sites exposure due to weaker Ag-SR bond than Au-SR bond based on DFT analysis; (3) weaker Ag-H than Au-H bond based on DFT analysis; and (4) better stability as smaller metal NCs during the catalytic reaction. The study reveals a wider opportunity to tailor the catalytic properties of atomically precise Au-based 25-metal atom NC by engineering its metal composition.

1. Introduction

Ultrasmall ligand-protected atomically precise metal nanoclusters (NCs) (size is less than 3 nm) have been increasingly studied in catalysis due to their atomic precision which allow more insights into their catalytic activity and mechanisms at molecular level. Among various metal NCs, gold (Au) is the most intensively made and studied as metal NCs. To date, increasing studies have reported excellent performance of Au NCs in various chemical transformations. These chemical transformations can be divided into several groups: (1) oxidation (*e.g.,* oxidation of styrene [1–8], benzyl alcohol [1,9], and CO [10–16] selective aerobic oxidation of amines to imines [17,18], selective oxidation of sulfide to sulfoxide [18,19], selective oxidation of styrene [20] and epoxidation of styrene [21]); (2) hydrogenation (*e.g.,* hydrogenation of 4-nitrophenol [22,23], nitrobenzene [2,24], nitrobenzonitrile [25], bicyclic ketone [26], semihydrogenation of alkyne [27] and chemoselective hydrogenation of nitrobenzaldehyde [28–30] and benzalacetone [5,31]); (3) coupling reactions (*e.g.,* Ullmann homocoupling reaction of aryl iodides [32], Ullmann heterocoupling reaction between iodobenzene and 4-nitro-iodobenzene [33], Sonogashira coupling reaction between iodobenzene and phenylacetylene [34] and Suzuki cross-coupling reaction between iodoanisole and phenylboronic acid [35]) and (4) electrocatalysis (*e.g.,* electrochemical water oxidation [36], oxygen reduction reaction [37] and CO_2 reduction [38]).

There are several methods to tailor the catalytic properties of Au NC catalysts, either by varying the ligands [39] or the metal composition [29,40]. Engineering metal composition of Au NCs has become a popular approach. It expands the scope of study and facilitates the understanding of physicochemical properties and application of Au NCs. One of the methods in engineering metal composition of Au NCs is varying the number of metal atom, further affecting the overall size of Au NCs and their catalytic properties. For example, it was reported that the catalytic activity of monometallic $Au_n(GSH)_m$ NCs (where GSH = glutathione ligand) in the chemoselective hydrogenation of 4-nitrobenzaldehyde to 4-nitrobenzyl alcohol followed the order of $Au_{38}(GSH)_{24} > Au_{25}(GSH)_{18} > Au_{18}(GSH)_{14} > Au_{15}(GSH)_{13}$, showing more Au atoms, higher catalytic activity [29]. However, in the oxidation of amines to imines, opposite effect of size on the catalytic activity of heterogeneous Au_{11}, Au_{25} and Au_{101} NCs was reported [41]. This opposite observation conveys that Au NCs of different size, may have different number of ligands, electronic and molecular structures which prominent to their catalytic properties. Hence, comparing the catalytic performances of Au

* Corresponding authors at: Department of Chemical and Biomolecular Engineering, National University of Singapore, 4 Engineering Drive 4, 117585 Singapore.
E-mail addresses: riccanasaruddin@iium.edu.my (R.R. Nasaruddin), chexiej@nus.edu.sg (J. Xie).

https://doi.org/10.1016/j.mcat.2021.112095
Received 15 September 2021; Received in revised form 10 December 2021; Accepted 23 December 2021
Available online 7 January 2022

NCs of different number of metal atoms could be challenging.

Alternatively, doping Au NCs with foreign metals which produces a class of bimetallic Au-based NCs, is another attractive method in engineering metal composition of Au NCs. Au-based bimetallic NCs have received increasing attention because more opportunities for tuning their physicochemical and catalytic properties are available. Several Au-based bimetallic NCs that have been reported are Au-silver (AuAg) [40,42–62], Au-copper (AuCu) [40,53,61–67], Au-platinum (AuPt) [40,68–70], Au-palladium (AuPd) [61,68], Au-manganese (AuMn) [71,72], Au-mercury (AuHg) [62,73,74], Au-cadmium (AuCd) [62,74–76] and Au-aluminium (AuAl) NCs [77]. Among them, AuAg NCs are the most intensively studied because Ag has a close similarity in electronic structure with Au ($d^{10}s^1$) [53] and Au NCs could readily reduce Ag(I) precursor [62]. Interestingly, bimetallic NCs can also be produced with different metal composition while maintaining similar number of total metal atoms and ligands, hence, the well-defined structure of NCs could be preserved [42,62]. For instance, mixtures of $Au_{25-x}Ag_x(SR)_{18}$ NCs (where SR = thiolate ligand and x = 1 – 11) were produced with different $R_{Au/Ag}$ feeding ratios by Dou et al. [42]. Meanwhile, Wang et al. had synthesized $Au_{25-x}M_x(SR)_{18}$ NCs with different type of metal dopants (*i.e.,* M = Ag, Cu, Cd and Hg), implying the robustness of Au NCs with 25-metal atom structure (or simplified as $Au_{25}(SR)_{18}$ NCs) [62]. Moreover, the effects of foreign metal dopants in the bimetallic 25-metal atom NCs can be well investigated because their skeletal structure was still similar to the original monometallic $Au_{25}(SR)_{18}$ NCs [60,78].

Several studies on Au-based bimetallic NCs with 25 metal atoms have been reported [40,58,69,70,75,79]. For instance, Yao et al. reported a higher catalytic activity of bimetallic $Au_{25}Ag_2(SR)_{18}$ NCs in hydrolyzing 1,3-diphenylprop-2-ynyl acetate than using monometallic $Au_{25}(SR)_{18}$ NCs [58]. But the structure of $Au_{25}Ag_2(SR)_{18}$ NC was not resolved and it could be different than $Au_{25}(SR)_{18}$ NC [58]. In another studies, bimetallic $Pt_1Au_{24}(SR)_{18}$ NCs gave higher conversion and selectivity to the oxidation of styrene to benzaldehyde than using $Au_{25}(SR)_{18}$ NCs [69]. $Pt_1Au_{24}(SR)_{18}$ NCs also exhibited higher activity in electrochemical production of hydrogen, as compared to the benchmark Pt/C catalyst [70]. Meanwhile, $Cd_1Au_{24}(SR)_{18}$ NCs had higher activity for aerobic oxidation of benzyl alcohol as compared to $Au_{25}(SR)_{18}$ NCs [75]. In addition, effects of different metal dopants was also reported in Sonogashira coupling reaction, which Ag_xAu_{25-x} $(SR)_{18}$ NCs gave slightly higher conversion than $Au_{25}(SR)_{18}$ NCs but Pt_xAu_{25-x} $(SR)_{18}$ and Cu_x-Au_{25-x} $(SR)_{18}$ NCs gave opposite results [40]. Higher activity of Au_{25-x}-$Ag_x(SR)_{18}$ than $Cu_xAu_{25-x}(SR)_{18}$ and $Au_{25}(SR)_{18}$ NCs was also reported in oxidation of styrene [79]. However, most of these reported studies used heterogeneous bimetallic and monometallic NCs. The NCs might have different structure after being immobilized onto support materials, hindering a better understanding on the relationships between their structure and catalytic properties.

Herein, we study the effects of silver doping to the catalytic properties of ligand-protected Au-based 25-metal NCs where the ligands are thiolates (*i.e.*, C_6-mercaptohexanoic acids (denoted as MHA)), without compromising the presence of ligands and the well-defined structure of 25-metal NC. Interestingly, it was found that the more Ag dopants in the $Au_{25-x}Ag_x(MHA)_{18}$ NCs, the better the accessibility and the catalytic activity of the bimetallic NCs than the monometallic $Au_{25}(MHA)_{18}$ NCs. The enhancement in the catalytic properties of $Au_{25-x}Ag_x(MHA)_{18}$ NCs might be originated from a combination of synergistic effects between Au and Ag atoms in the 25-metal NCs, the interaction between the Au and Ag atoms with the MHA ligands and hydrides and the stability of the NCs during the catalytic reaction.

2. Experimental section

2.1. Materials

Ultrapure Millipore water (18.2 MΩ) was used throughout the experiment. All glassware were washed with aqua regia, rinsed with copious water and then ethanol and dried in an oven before use. Hydrogen tetrachloroaurate(III) hydrate ($HAuCl_4{\cdot}3H_2O$) from Alfa Aesar; Sodium borohydride ($NaBH_4$), C_6-mercaptohexanoic acid (MHA) and 4-nitrophenol from Sigma-Aldrich; sodium hydroxide (NaOH) and silver nitrate ($AgNO_3$) from Merck; were used as received.

2.2. Synthesis of $Au_{25-x}Ag_x(MHA)_{18}$ NCs

Synthesis of $Au_{25-x}Ag_x(MHA)_{18}$ NCs was made by using NaOH-mediated $NaBH_4$ reduction method as reported by Dou et al. [42] but with a minor modification. Briefly, an aqueous solution of MHA (5 mM, 2 mL) was first mixed with water (2.25 mL), followed by adding 0.25 mL mixture of $HAuCl_4$ (20 mM) and $AgNO_3$ (20 mM). The different feeding ratios of Au^{3+}/Ag^+ or $R_{Au/Ag}$ were 25/0 (Au precursor only), 24/1, 22/3 and 18/7. The synthesis was done under rigorous stirring (500 rpm), leading to the formation of Au(I)/Ag(I)-MHA complexes. Both gold and silver precursors were co-reduced in this synthesis method. Aqueous solutions of NaOH (1 M, 0.3 mL) and $NaBH_4$ (~112 mM, 0.2 mL, prepared by dissolving 43 mg of $NaBH_4$ powder in 10 mL of 0.2 M NaOH solution) were then separately added to the reaction mixture. The $Au_{25-x}Ag_x(MHA)_{18}$ NCs were collected after 3 h of reaction. The as-prepared samples were centrifuged and purified using PD10 desalting column.

2.3. Characterization of $Au_{25-x}Ag_x(MHA)_{18}$ NCs

The purified products were characterized by UV-Vis spectrometry (Shimadzu UV-1800 spectrometer) and electrospray ionization mass spectrometry, ESI-MS (Bruker microTOF-Q system in the negative ion mode). Detailed operating conditions of ESI-MS analysis were as follows: source temperature/100 °C, dry gas flow rate/4 L per min, nebulizer pressure/2 bar and capillary voltage/3.5 kV. In a typical ESI-MS analysis, 0.1 mL of sample was injected with a flow rate of 180 μL/h. The Au and Ag contents were determined by inductively coupled plasma mass spectrometry (ICP-OES) on an Agilent 7500A. The oxidation state of Au and Ag was analyzed by X-ray photoelectron spectrometry (XPS) which was conducted on a Kratos AXIS UltraDLD spectrometer.

2.4. Catalytic test of 4-nitrophenol hydrogenation

Hydrogenation of 4-nitrophenol ($C_6H_5NO_3$) to 4-aminophenol by $NaBH_4$ ($C_6H_5ONH_2$) in solution was carried out at room temperature. In a typical catalytic reaction, 4-nitrophenol (4 mM, 30 μL) was introduced into the catalysts (~30.8 μM of metal content, 10 μL) in a 3 mL quartz cuvette. After that, excess $NaBH_4$ (0.018 M, 1.46 mL) was added to initiate the reduction. The catalytic reaction in the cuvette was then analyzed by UV-Vis spectrometry. The amount of $NaBH_4$ was corresponding to 200x more than the stoichiometric requirement in 4-nitrophenol hydrogenation as shown follow:

$$4\ C_6H_5NO_3 + 3\ NaBH_4 \rightarrow 4\ C_6H_5ONH_2 + 3\ NaBO_2 + 2\ H_2O$$

2.5. DFT calculations

Metal NCs' geometries and energies were simulated on the M06L level of theory using 6–31 G as a basis set for carbon, hydrogen and sulfur atoms and LANL2DZ and the corresponding LANL2DZ effective core potentials for Au and Ag. All calculations were carried out using Gaussian 16 Rev. A.03 and the structures were plotted using Avogadro. Marenich et al. analysis was performed using the Charge Model 5 extended Hirshfeld population analysis [80]. Initial geometries were extracted from the $Au_{25}(SR)_{18}$ NC's crystal structure [81]. The aromatic thiolate ligands were approximated by methanethiolate (SCH_3) ligands in order to save computation time. It was shown before that the exact

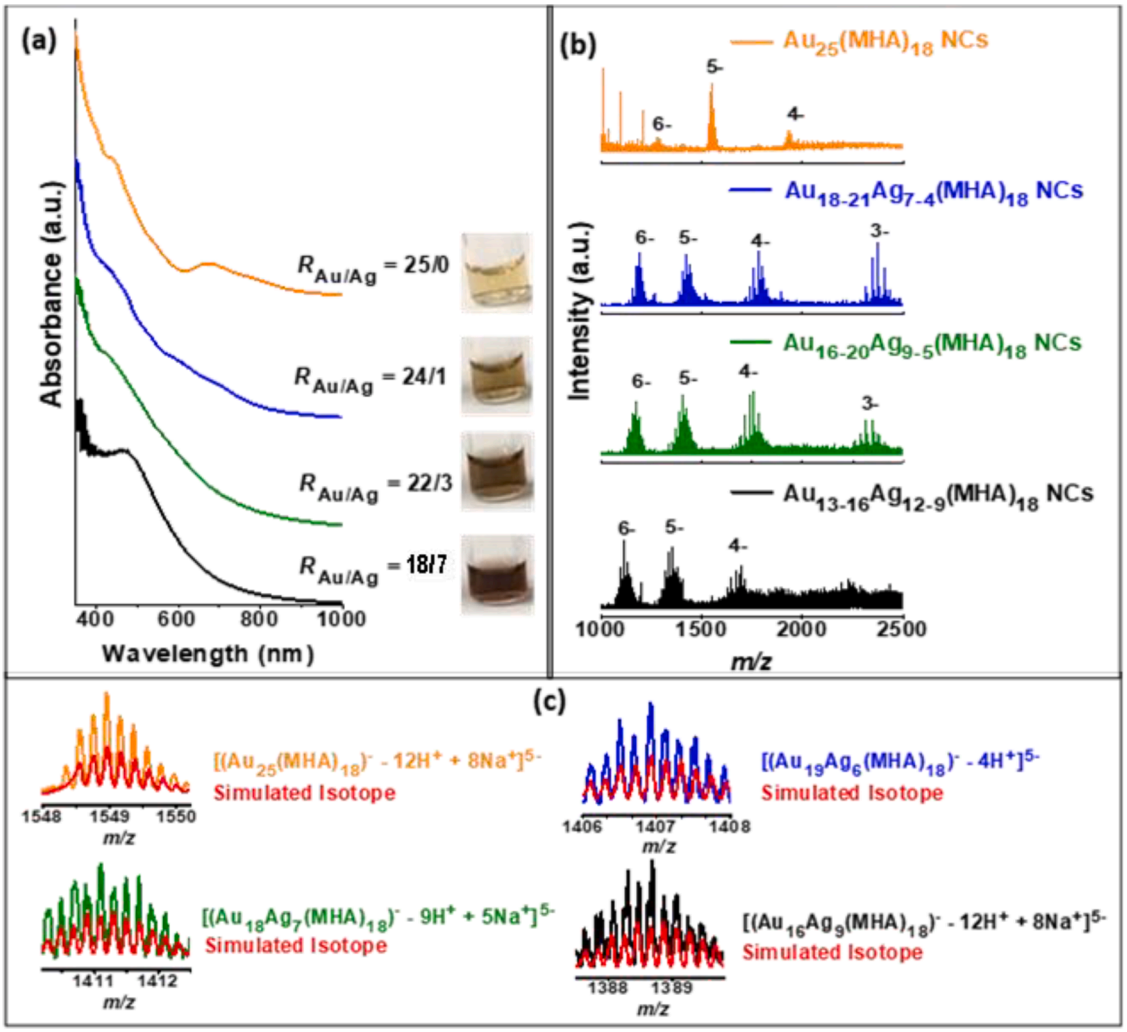

Fig. 1. Characterization of the purified catalysts. (a) UV-Vis absorption spectra of the $Au_{25}(MHA)_{18}$ NCs and $Au_{25-x}Ag_x(MHA)_{18}$ NCs and the insets show the color of the NCs solutions. (b) ESI mass spectra of $Au_{25}(MHA)_{18}$ NCs and $Au_{25-x}Ag_x(MHA)_{18}$ NCs. (c) ESI mass spectra and simulated isotope patterns of an identified species of each NCs.

structure of the thiolate ligands does not affect the calculation results significantly [82]. Nanoclusters were all assumed to be in a singlet, single negatively charged initial state before reaction. Reaction energies were estimated using the following formula (E denotes energy):

$$E_{reaction} = E_{products} - E_{reactants}$$

3. Results and discussion

3.1. Characterizations of $Au_{25}(MHA)_{18}$ NCs and $Au_{25-x}Ag_x(MHA)_{18}$ NCs

Monometallic $Au_{25}(MHA)_{18}$ NCs ($R_{Au/Ag}$= 25/0) displayed common characteristic peaks of Au_{25} NCs (at ~440, ~550, ~670 and ~760 nm) (Fig. 1a). The ESI mass spectrum of the NCs further confirmed the presence of $Au_{25}(MHA)_{18}$ NCs (orange line, Fig. 1b, c). The major identified species was $[(Au_{25}(MHA)_{18})^{-} - 12H^{+} + 8Na^{+}]^{5-}$ NC, indicating the presence of negatively charged $Au_{25}(MHA)_{18}^{-}$ NC with Na^{+} as counterion. Meanwhile, the UV-Vis absorption of $Au_{25-x}Ag_x(MHA)_{18}$ NCs was different from that of $Au_{25}(MHA)_{18}$ NCs (Fig. 1a) due to the presence of Ag atoms. Hence, the confirmation of 25-metal composition in $Au_{25-x}Ag_x(MHA)_{18}$ NCs was obtained from the ESI mass spectra (blue, green and black lines in Fig. 1b). The $R_{Au/Ag}$ feeding ratio of 24/1, 22/3 and 18/7 had produced mixtures of $Au_{18-21}Ag_{7-4}(MHA)_{18}$, $Au_{16-20}Ag_{9-5}(MHA)_{18}$ and $Au_{13-16}Ag_{12-9}(MHA)_{18}$ NCs, respectively. Interestingly, all the $Au_{25-x}Ag_x(MHA)_{18}$ NCs had similar 25 metal atoms and protected by similar 18 MHA ligands, indicating the Ag atoms replaced the Au atoms in making the NCs and all the bimetallic 25-metal atom NCs could have as similar geometrical structure as $Au_{25}(SR)_{18}$ NC [42]. The ESI mass spectra of the identified species of all the NCs matched well with their simulated isotope patterns in Fig. 1c, and Figs. S1–S3 (Supplementary Material†), confirming their molecular formulas.

When the feeding ratio of Ag ($R_{Au/Ag}$) was increased from 24/1 to 22/3 and 18/7, the electronic property of $Au_{25-x}Ag_x(MHA)_{18}$ NCs differed significantly from $Au_{25}(MHA)_{18}$ NCs as the UV-Vis absorption peak at ~670 nm of $Au_{25-x}Ag_x(MHA)_{18}$ NCs almost disappeared (Fig. 1a). The characteristic UV-Vis absorption peak at ~670 nm corresponds to HOMO-LUMO transition which associated with the electronic and geometric structure of Au_{13} icosahedral core in the structure of $Au_{25}(SR)_{18}$ NC [58]. The disappearance of this peak reveals that the electronic property of Au_{13} core was affected by the Ag dopants. Meanwhile, the characteristic peak at ~440 nm corresponds to the mixed intraband ($sp \leftarrow sp$) and interband ($sp \leftarrow d$) transitions, which associated with the Au_{12} located in the exterior staple motifs of $Au_{25}(SR)_{18}$ NC skeleton. As can be seen in Fig. 1a, this peak started to disappear at the highest feeding ratio of Ag (R_{Au-Ag} = 18/7), indicating

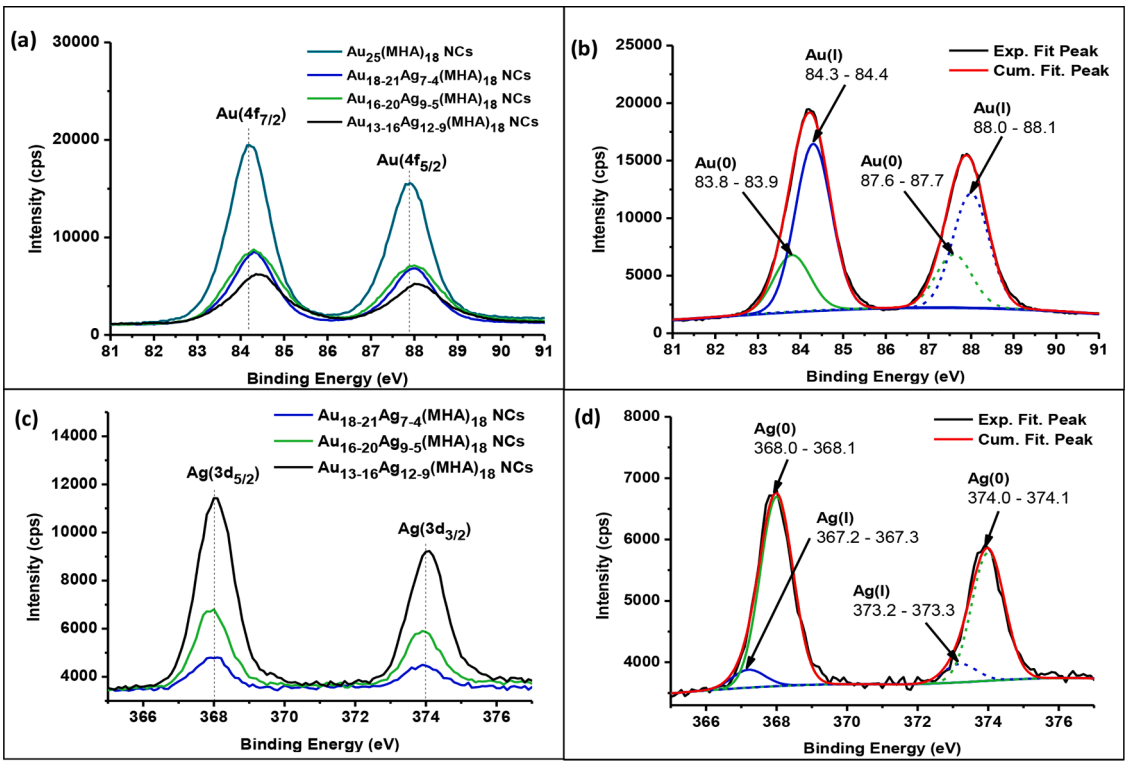

Fig. 2. (a) XPS spectra for Au(4f) of $Au_{25}(MHA)_{18}$ and $Au_{25-x}Ag_x(MHA)_{18}$ NCs. (b) Deconvoluted XPS spectra of Au(4f) peaks of $Au_{25}(MHA)_{18}$ NCs as an example. (c) XPS spectra of Ag(3d) of $Au_{25-x}Ag_x(MHA)_{18}$ NCs. (d) Deconvoluted XPS spectra for Ag(3d) of $Au_{16-20}Ag_{9-5}(MHA)_{18}$ NCs as an example.

Table 1
Percentage of Au(0), Au(I), Ag(0) and Ag(I) in the catalysts.

Catalysts	Total (%)		Total (%)	
	Au(0)	Au(I)	Ag(0)	Ag(I)
$Au_{25}(MHA)_{18}$ NCs	28.0	72.0	0	0
$Au_{18-21}Ag_{7-4}(MHA)_{18}$ NCs	5.7	94.3	86.0	14.0
$Au_{16-20}Ag_{9-5}(MHA)_{18}$ NCs	4.5	95.5	89.7	10.3
$Au_{13-16}Ag_{12-9}(MHA)_{18}$ NCs	3.5	96.5	91.5	8.5

the Au atoms at staple motif were also affected by the highest amount of Ag dopants [58].

XPS analysis was performed to determine the possible locations of Ag dopants in the geometrical structure of $Au_{25-x}Ag_x(MHA)_{18}$ NCs (Fig. 2). The XPS peak centered at ~84.2 eV and ~88.0 correspond to Au($4f_{7/2}$) and Au($4f_{5/2}$), respectively (Fig. 2a) [44,83]. When the amount of Ag dopants increased, these peaks shifted to higher binding energy because the electron density of Au(4f) has been withdrawn [44], probably to reduce the Ag(I) and/or Ag(I)-MHA complexes. These peaks can be further deconvoluted using the Gaussian function with identical full width at half minimum (FWHM). The deconvoluted peaks centered at 83.8–83.9 eV and 87.6–87.7 eV are attributed to Au(0) while the deconvoluted peaks centered at 84.3–84.4 eV and 88.0–88.1 eV are attributed to Au(I) (Fig. 2b).

On the other hand, Fig. 2c shows the XPS spectra for Ag(3d) for $Au_{25-x}Agx(MHA)_{18}$ NCs. The peaks centered at ~368.0 eV and ~374 eV denote Ag(3d5/2) and Ag(3d3/2), respectively [44,59,62]. These XPS peaks also shifted slightly to higher binding energy when the silver dopants increased. To determine the oxidation state of the silver dopants in the $Au_{25-x}Ag_x(MHA)_{18}$ NCs, these peaks can be further deconvoluted. The deconvoluted peaks centered at 368.0–368.1 and 374.0–374.1 are attributed to Ag(0) while the deconvoluted peaks centered at 367.2–367.3 and 373.2–373.3 are attributed to Ag(I) (Fig. 2d) [44,59,62]. Figs. S4 and S5 shows the deconvoluted XPS spectra of Au(4f) and Ag(3d) of other bimetallic NCs, respectively. The percentage of Au(0), Au(I), Ag(0) and Ag(I) in all NCs based on the deconvoluted results were summarized in Table 1.

In the superatom model of $[Au_{25}(SR)_{18}]^-$ NC, there are eight electron counts and the $[Au_{25}(SR)_{18}]^-$NC has Au_{13}^{5+} icosahedral core which consists of five Au(I) and eight Au(0) [84]. This core is protected by six staple motifs (-SR-Au(I)-SR-Au(I)-SR-), which overall contains twelve Au (I) [5,82,85]. Therefore, with total seventeen Au(I) and eight Au(0), it was predicted that 68% will be Au(I) and 32% will be Au(0). The deconvolution of XPS spectra resulted in 72% of Au(I) and 28% of Au(0) in $Au_{25}(MHA)_{18}$ NCs, which were close to the predicted values (Table 1). When Ag dopants were introduced and increased in $Au_{25-x}Ag_x(MHA)_{18}$ NCs, the percentage of Au(I) increased and the percentage of Au(0) decreased, indicating the remaining Au species in the bimetallic NCs were mainly at the staple motif rather than the icosahedral core. Oppositely, the percentage of Ag(I) decreased and the percentage of Ag (0) increased, indicating that most of Ag species were replacing Au(0) at the icosahedral core, becoming Ag(0) (Fig. S6) which similar to existing reported studies [59,62].

In addition, based on reported density functional theory (DFT), overall substitution reaction for both Ag atoms and Ag(I)-SR complex were exothermic, which referred to the lowering of total energy by inclusion of Ag(I)-SR complex into $Au_{25}(SR)_{18}$ NC [54]. The same study also revealed that the overall reaction energies (ΔE) for Ag atom at the vertex of the icosahedral core was + 0.23 eV, lower than that at central atom (+ 0.71 eV) and staple motif (+0.44 eV)[54]. Therefore, the Ag atoms prefer to stay in the vertex position of the icosahedral Au_{13} core of $Au_{25-x}Ag_x(SR)_{18}$ NC [53,54]. The reported information justifies similar findings in this study. The observations in previous UV-Vis absorption spectra (Fig. 1a) can also justify the preferred location of Ag dopants in $Au_{25-x}Ag_x(SR)_{18}$ NC. When comparing the UV-Vis absorption peak at ~670 nm (associated with the icosahedral core) and ~440 nm (associated with the staple motifs), the disappearance of the peak at ~670 nm happened at lower Ag dopants ($R_{Au/Ag}$ = 22/3) as compared to that for peak at ~440 nm ($R_{Au/Ag}$ = 18/5). Therefore, the Ag dopants prefer to

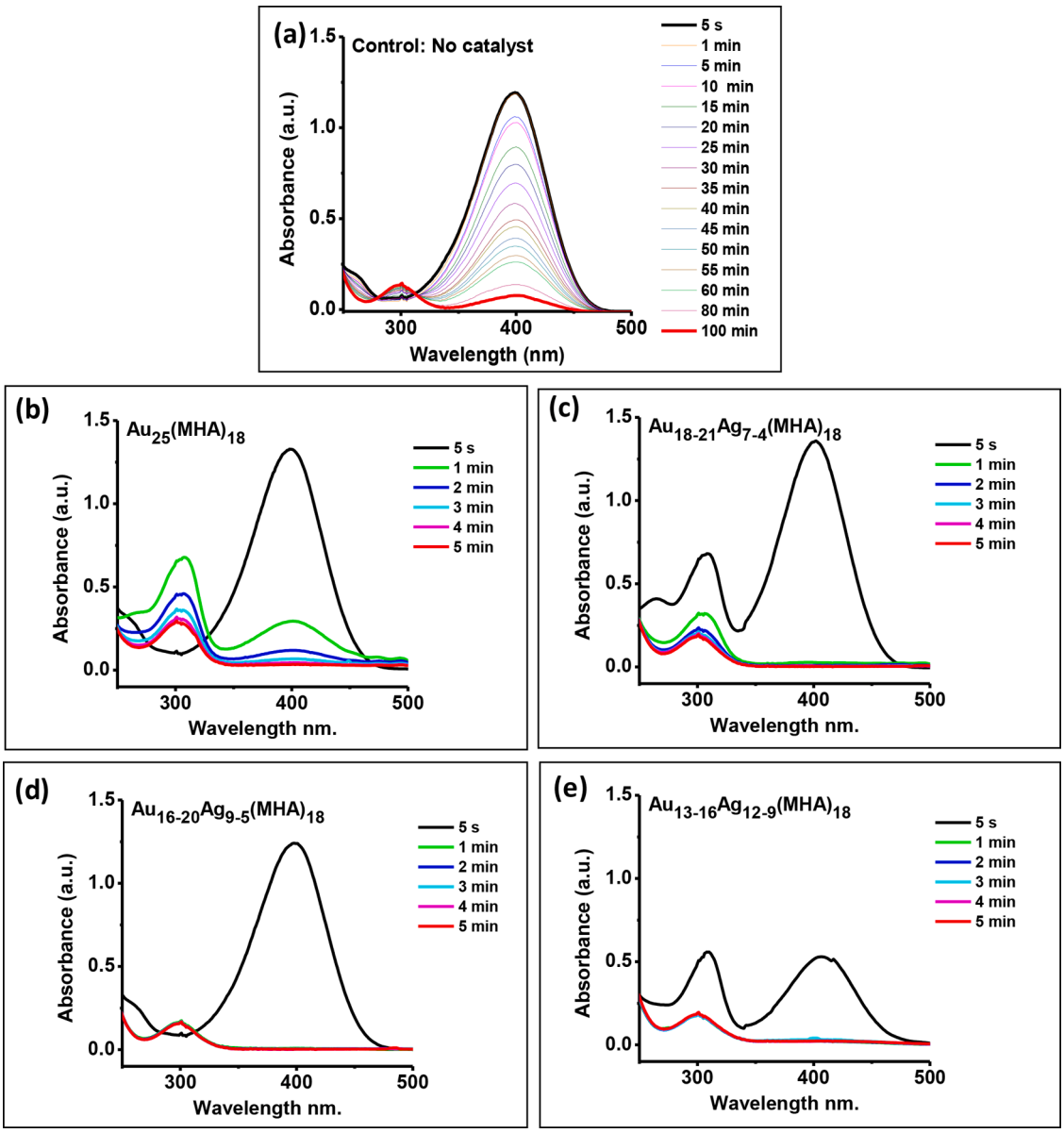

Fig. 3. Time-evolution UV-Vis absorption spectra of 4-nitrophenol hydrogenation using $NaBH_4$ as reducing agent (a) without catalyst (control experiment) and (b–e) with the presence of catalysts ($Au_{25}(MHA)_{18}$ and $Au_{25-x}Ag_x(MHA)_{18}$ NCs).

replace Au atoms at the vertex of Au_{13} icosahedral core or stay at that location, thus affecting the electronic property at ~670 nm.

3.2. Catalytic test: 4-nitrophenol hydrogenation

The catalytic performance of the $Au_{25}(SR)_{18}$ NCs and $Au_{25-x}Ag_x(SR)_{18}$ NCs was further tested using hydrogenation of 4-nitrophenol in solution as the model reaction due to its simplicity. Control experiment (without any catalyst) gave > 90% conversion, only after 100 min of reaction (Fig. 3a). However, in the presence of catalysts, the rate of reaction was significantly increased, and 100% conversion was achieved within 5 min of reaction (Fig. 3b–e).

To compare the performance of each catalyst, the accessibility (*i.e.*, based on the induction time, t_0) and the catalytic activity (*i.e.*, based on the apparent reaction rate constant, k_{app}) were determined by analyzing the UV-Vis absorption at 400 nm under kinetic mode (Fig. 4). As shown in Fig. 4, the addition of Ag dopants had enhanced the catalytic activity of $Au_{25-x}Ag_x(SR)_{18}$ NCs based on the increasing k_{app} values, from 0.04 s^{-1} for $Au_{25}(MHA)_{18}$ NCs to 0.07 s^{-1} for $Au_{18-21}Ag_{7-4}(MHA)_{18}$ NCs, 0.15 s^{-1} for $Au_{16-20}Ag_{9-5}(MHA)_{18}$ NCs and 0.28 s^{-1} for $Au_{13-16}Ag_{9-6}(MHA)_{18}$ NCs. Interestingly, the addition of Ag dopants also enhanced the accessibility of the catalysts based on the decreasing t_0 values, although all the catalysts are protected by the same MHA ligands. Therefore, it can be speculated that the activation of the catalysts occurred at a different time and might not depend only on the diffusion of substrates through the ligands shell [86]. The activation of the reaction might also include ligand's removal and structural transformation of the NC catalysts as recently reported by Nasaruddin et al. [87]. It shows that the interaction of thiolate to Au and Ag was different, thus, the accessibility of each of the catalysts was non-identical although they were protected by the same MHA ligands.

3.3. Factors affecting the enhancement of catalytic activity by Ag dopants

The factors for the enhancement of catalytic properties of $Au_{25-x}Ag_x(MHA)_{18}$ NCs as compared to $Au_{25}(MHA)_{18}$ NCs could be resulted from a combination of several factors. As compared to monometallic $Au_{25}(SR)_{18}$ NCs, $Au_{25-x}Ag_x(SR)_{18}$ NCs have (1) synergistic effects of Au

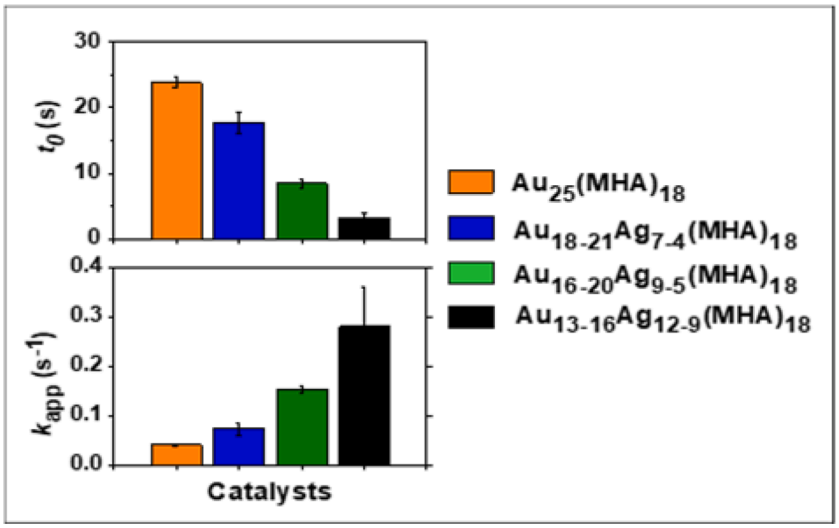

Fig. 4. Induction time (t_0) and apparent reaction rate constant (k_{app}) of the catalysts ($Au_{25}(MHA)_{18}$ and $Au_{25-x}Ag_x(MHA)_{18}$ NCs).

and Ag atoms; (2) better ligands removal's and active sites exposure due to weaker Ag-SR bond than Au-SR bond based on DFT analysis; (3) weaker Ag-H than Au-H bond based on DFT analysis; and (4) better stability as smaller metal NCs. For the first factor (synergistic effects), it has been reported that the catalytic activity of Ag NCs was lower than that of Au NCs in the hydrogenation of 4-nitrophenol in solution using $NaBH_4$ as reducing agent [88]. Therefore, by replacing the Au active sites with Ag active sites in $Au_{25-x}Ag_x(MHA)_{18}$ NCs, the catalytic activity is expected to be lower. However, in this study, the combination of Au and Ag atoms had increased the catalytic activity of the $Au_{25-x}Ag_x(MHA)_{18}$ NCs as compared to $Au_{25}(MHA)_{18}$ NCs in 4-nitrophenol hydrogenation, indicating the presence of synergistic effects between the Au and Ag atoms in the bimetallic NCs. It was reported from a computational study that Au atoms could attract electron density from Ag and consequently, Ag behaves as good acceptors for electrons, showing the presence of synergistic effects between the Au and Ag in an alloy system [89], which could also happened in the bimetallic $Au_{25-x}Ag_x(MHA)_{18}$ NCs. Higher activity of bimetallic AuAg NCs than Au NCs was also reported in other catalytic reactions [40,79].

Secondly, several studies have reported that the removal of thiolate ligands was responsible for activating the catalytic reaction of the metal NC catalysts [87,90–92]. Therefore, the higher catalytic activity of $Au_{25-x}Ag_x(MHA)_{18}$ NCs when the silver dopants increased could be due to the easier desorption of thiolate from the NCs, allowing more metal active sites exposure for the catalytic reaction. It is well known that the bond between Au and thiolate (Au-SR) is stronger than the bond between Ag and thiolate (Ag-S). Based on reported computational study, the binding energy of individual Au-S and Ag-S are −6.79 kcal/mol and 2.22 kcal/mol, respectively. Moreover, the Au-S binding energy decreases by the increasing of Ag in AuAg alloy [89]. Therefore, DFT analysis was done to justify the weaker bonding between the metal and ligands in $Au_{25}(MHA)_{18}$ NCs and $Au_{25-x}Ag_x(MHA)_{18}$ NCs. The calculation was done on the reported crystal structures of thiolated Au_{25} NC but the more complex aromatic thiolate ligands were replaced by methylthiolate (SCH_3) in order to simplify the structures [82]. A Hirshfeld population analysis on Au_{25}, $Au_{19}Ag_6$ and $Au_{13}Ag_{12}$ clusters revealed that there is indeed an increase in the average positive charge on the Au atoms upon substitution of 6 or 12 of the Au atoms at the icosahedral core by Ag atoms (Table S1) well in accordance with the shift towards higher binding energies observed by XPS analysis. Similarly, the average charge of Ag was shown to decrease upon substitution of more Au atoms by Ag atoms.

Besides confirming the changed electronic state of the bimetallic NCs, we modeled the thermodynamics of the ligand removal and substitution by hydride ions from Au_{25} and $Au_{13}Ag_{12}$ NCs. We considered the removal and replacement of thiolate ligands from two positions on the staple motif (position A and B in Fig. 5a). It was found that the removal of thiolate ligands from both NCs was highly unfavorable and requires more than 500 kJ/mol in all cases considered. This accounts for the relatively high stability of the nanoclusters in the absence of sodium borohydride. Only upon addition of hydride species, the thiolate ligands can be removed favorably as shown in Fig. 5b which evidenced experimentally in reported study by Nasaruddin et al. [87]. In the same study, it was also found that the removal of Au-SR complexes was also responsible in activating the catalytic reaction. Thus, the catalytic activity of the $Au_{25-x}Ag_x(MHA)_{18}$ NCs may also be activated by the removal of Au-MHA, Ag-MHA or AuAg-MHA complexes.

The third enhancement factor is related to the bonding between the

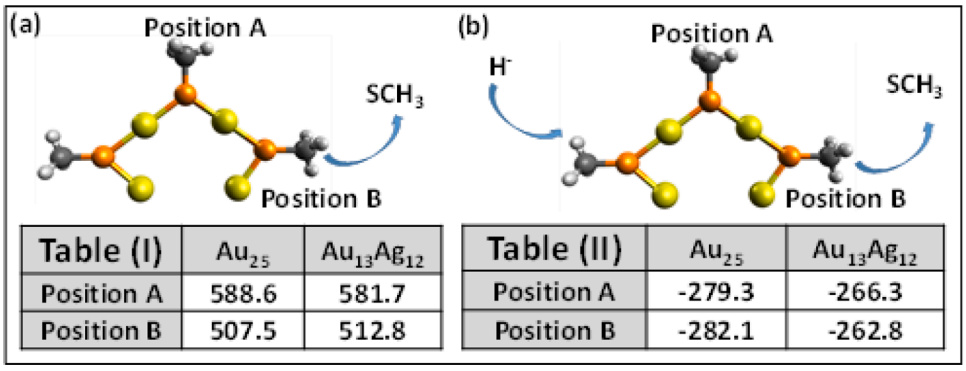

Table (I)	Au_{25}	$Au_{13}Ag_{12}$
Position A	588.6	581.7
Position B	507.5	512.8

Table (II)	Au_{25}	$Au_{13}Ag_{12}$
Position A	-279.3	-266.3
Position B	-282.1	-262.8

Fig. 5. Thermodynamic analysis of ligand (SCH_3) removal from the staple motif of $Au_{25}(SR)_{18}$ NCs and $Au_{13}Ag_{12}(SR)_{18}$ NCs (a) without the presence of hydride and (b) with the presence of hydride. Table (I) in (a) shows the energies (in kJ/mol) for the removal of methylthiolate from the two different positions in the staple motif for Au_{25} and $Au_{13}Ag_{12}$ nanoclusters and Table (II) in (b) shows the energies (in kJ/mol) for the substitution of methylthiolate by hydride from the two different positions in the staple motif for Au_{25} and $Au_{13}Ag_{12}$ nanoclusters.

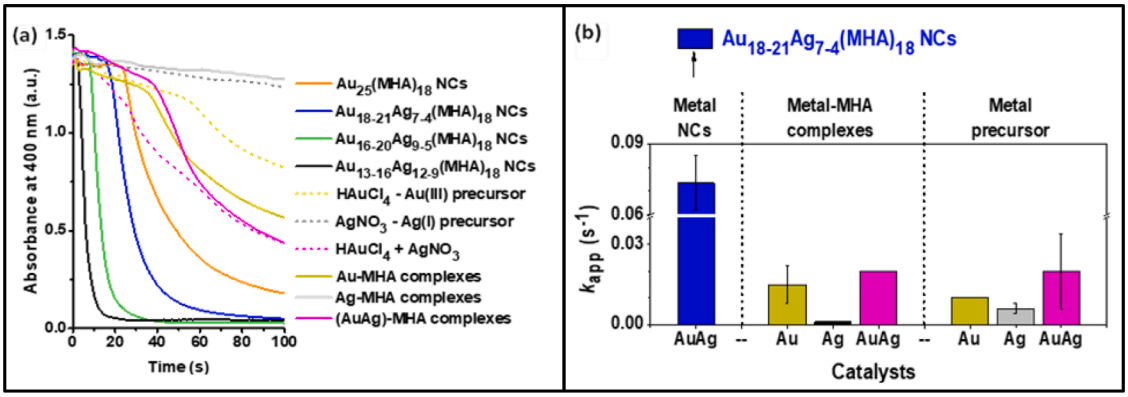

Fig. 6. (a) UV-Vis absorption spectra at 400 nm (kinetic mode) for the catalysts. (b) The apparent reaction rate constant (k_{app}) of selected $Au_{25-x}Ag_x(MHA)_{18}$ NCs ($Au_{18-21}Ag_{7-4}(MHA)_{18}$ NCs) as compared to their complexes and precursor.

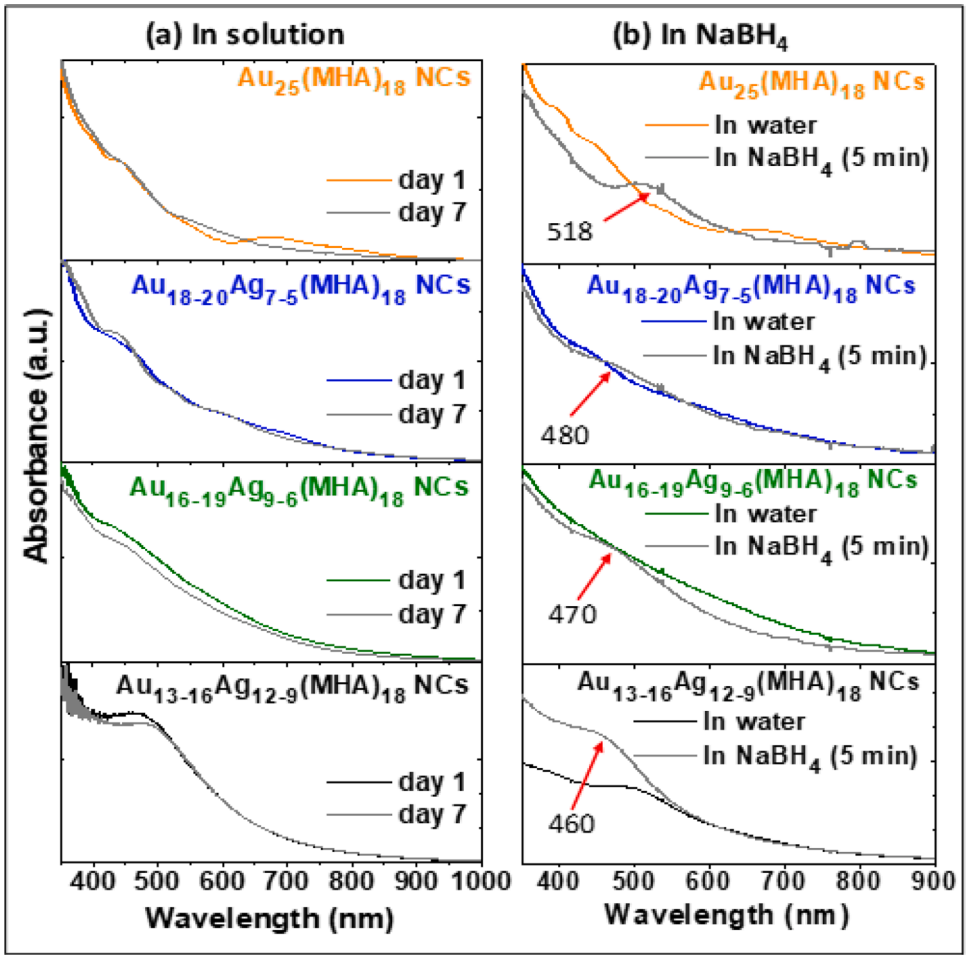

Fig. 7. Stability of $Au_{25}(MHA)_{18}$ NCs and $Au_{25-x}Ag_x(MHA)_{18}$ NCs based on UV-Vis absorption spectra (a) in water solution after 7 days and (b) after the water solution was mixed with $NaBH_4$. Mixture contains $NaBH_4$ (1.46 mL, 0.018 M) and NCs (0.2 mL, ~30.8 μM of metal content).

noble metal and hydrides. In the hydrogenation of 4-nitrophenol, hydrides play pivotal role as the reducing agent that convert 4-nitrophenol into 4-aminophenol. We had evidenced the presence of Au-H bonds on the Au NCs in our previous reported study [93,94]. The formation of Ag-H bond in hydride-rich Ag NCs has been also reported by Bootharaju et al. recently [95]. These Au-H and Ag-H are reported as the active sites for the hydrogenation of 4-nitrophenol [88]. Due to relativistic effects of Au, the Ag-H bond is also weaker than Au-H bond [96]. The weaker metal-hydride bond is preferable for the catalytic reaction because the transfer of electron and/or hydrides would be easier than the excessively strong metal-hydrides bonds which would also poison the metal active sites by pre-occupation [97]. The adsorption of hydrides on Ag could also be easier in the presence of synergistic effects between the Ag and Au in the bimetallic NCs as compared to that of mono-Au or mono-Ag catalysts [89].

The fourth factor is related to the stability of the catalysts. We first compared the catalytic activity of the catalysts with smaller metal-ligand complex, synthesized with no addition of NaBH4 (*i.e.,* Au-MHA,

Ag-MHA and (AuAg)-MHA complexes) and metal precursor (*i.e.,* $HAuCl_4$, $AgNO_3$ and the mixture of $HAuCl_4$ and $AgNO_3$) to determine the importance of NCs to the catalytic property of the catalysts. The results in Fig. 6a, b show that the NCs are the most catalytically active structure for the catalytic reaction because the catalytic activity of NCs was higher than that of metal precursor and metal-ligands complexes.

Then, we analyzed the stability of the catalysts in water and in $NabH_4$ solution. It was found that $Au_{25-x}Ag_x(MHA)_{18}$ NCs in solution were slightly stable than $Au_{25}(MHA)_{18}$ NCs after a week, probably because the synergistic effects between Au and Ag had altered the electronic structure and stability of $Au_{25-x}Ag_x(MHA)_{18}$ NCs (Fig. 7a). A computational analysis in another study also reported that alloying Au and Ag could enhance the stability of bimetallic NCs (*i.e.,* $Au_{31}Ag$ NCs) as compared to monometallic Au NCs (*i.e.,* Au_{32} NCs) [49]. Therefore, we further analyzed the stability of the catalysts when mixed with $NaBH_4$ to mimic the reaction condition. Reactant, 4-nitrophenol was not added to avoid disturbance by the UV-Vis absorption peak at ~400 nm (due to the presence 4-nitrophenolate ions). The amount of all NCs was also increased from 0.01 mL to 0.2 mL to increase its visibility under the UV-Vis absorption analysis.

After 5 min mixed with $NaBH_4$, there was a distinctive surface plasmon resonance (SPR) band at ~518 nm for $Au_{25}(MHA)_{18}$ NCs, indicating that the $Au_{25}(MHA)_{18}$ NCs could be aggregated into bigger Au NPs during the catalytic reaction (Fig. 7b). This observation is consistent with the reported study by Li et al. [93,94]. They found that one the final fates of Au NCs during similar reaction was their conversion into bigger size NCs [93,94]. On the other hand, for each $Au_{25-x}Ag_x(MHA)_{18}$ NCs, a blue shifted shoulder peak was observed. This peak shifted more to higher energy band (lower wavelength) when the Ag dopants increased (from ~480 to ~460 nm). These shoulder peaks could belong to a mixture of AuAg NCs and smaller AuAg NPs (~4 nm) [93,94], indicating that $Au_{25-x}Ag_x(MHA)_{18}$ NCs were more stable as NCs or smaller NPs during the catalytic reaction. As NCs and smaller NPs have higher surface area-to-volume ratio, thus they are more reactive for catalysis as compared to Au NPs transformed from $Au_{25}(MHA)_{18}$ NCs.

4. Conclusion

We have studied the effects of silver (Ag) doping to the catalytic properties of Au NCs without compromising the presence of ligands and the structure of 25-metal atom NC. The findings show that the catalytic properties of bimetallic $Au_{25-x}Ag_x(SR)_{18}$ NCs were better than $Au_{25}(SR)_{18}$ NCs due to combination of several factors. As compared to monometallic $Au_{25}(SR)_{18}$ NCs, $Au_{25-x}Ag_x(SR)_{18}$ NCs have (1) synergistic effects of Au and Ag atoms; (2) better ligands removal's and active sites exposure due to weaker Ag-SR bond than Au-SR bond based on DFT analysis; (3) weaker Ag-H than Au-H bond based on DFT analysis; and (4) better stability as smaller metal NCs. The DFT analysis justifies the removal of ligands for higher exposure of the active sites is much easier with the presence of Ag dopants in the NCs structure and hydrides in the solution. The study reveals a wider opportunity to tailor the catalytic activity of atomic precision and well-defined structure metal NCs via engineering metal composition of metal NCs and study their catalytic properties at molecular level.

CRediT authorship contribution statement

Ricca Rahman Nasaruddin: Conceptualization, Methodology, Formal analysis, Writing – original draft. **Max J. Hülsey:** Formal analysis, Writing – review & editing. **Jianping Xie:** Supervision, Conceptualization, Writing – original draft.

Declaration of Competing Interest

There are no conflicts of interest to declare.

Acknowledgment

The authors acknowledge financial support from Ministry of Education, Singapore under grant number R-279–000–538–114. R.R. Nasaruddin acknowledges the financial support from the Ministry of Higher Education for his Ph.D. study at National University of Singapore. She also would like to acknowledge the financial support from the IIUM Research Acculturation Grant Scheme under grant number IRAGS18–024–0025 for the continuation of this study at IIUM.

Supplementary materials

Supplementary material associated with this article can be found, in the online version, at doi:10.1016/j.mcat.2021.112095.

References

[1] B. Zhang, J. Fang, J. Li, J.J. Lau, D. Mattia, Z. Zhong, J. Xie, N. Yan, Oxidative Stripping of Alkyl Thiolate Ligands from Hydroxyapatite-Supported Gold Nanoclusters for Oxidation Reactions, Chem. Asian. J. 11 (2016) 532–539.
[2] J. Fang, J. Li, B. Zhang, X. Yuan, H. Asakura, T. Tanaka, K. Teramura, J. Xie, N. Yan, The support effect on the size and catalytic activity of thiolated Au_{25} nanoclusters as precatalysts, Nanoscale 7 (2015) 6325–6333.
[3] Y. Liu, H. Tsunoyama, T. Akita, S. Xie, T. Tsukuda, Aerobic Oxidation of Cyclohexane Catalyzed by Size-Controlled Au Clusters on Hydroxyapatite: Size Effect in the Sub-2 nm Regime, ACS Catal. 1 (2011) 2–6.
[4] L. Li, S. Huang, J. Song, N. Yang, J. Liu, Y. Chen, Y. Sun, R. Jin, Y. Zhu, Ultrasmall Au_{10} clusters anchored on pyramid-capped rectangular TiO_2 for olefin oxidation, Nano Res. 9 (2016) 1182–1192.
[5] Y. Zhu, H. Qian, M. Zhu, R. Jin, Thiolate-protected Au_n nanoclusters as catalysts for selective oxidation and hydrogenation processes, Adv. Mater. 22 (2010) 1915–1920.
[6] Y. Zhu, H. Qian, R. Jin, An Atomic-Level Strategy for Unraveling Gold Nanocatalysis from the Perspective of $Au_n(SR)_m$ Nanoclusters, Chem. Eur. J. 16 (2010) 11455–11462.
[7] P. Huang, G. Chen, Z. Jiang, R. Jin, Y. Zhu, Y. Sun, Atomically precise Au_{25} superatoms immobilized on CeO_2 nanorods for styrene oxidation, Nanoscale 5 (2013) 3668–3672.
[8] C. Liu, S. Lin, Y. Pei, X.C. Zeng, Semiring chemistry of $Au_{25}(SR)_{18}$: fragmentation pathway and catalytic active site, J. Am. Chem. Soc. 135 (2013) 18067–18079.
[9] H. Tsunoyama, H. Sakurai, Y. Negishi, T. Tsukuda, Size-Specific Catalytic Activity of Polymer-Stabilized Gold Nanoclusters for Aerobic Alcohol Oxidation in Water, J. Am. Chem. Soc. 127 (2005) 9374–9375.
[10] J. Good, P.N. Duchesne, P. Zhang, W. Koshut, M. Zhou, R. Jin, On the functional role of the cerium oxide support in the $Au_{38}(SR)_{24}/CeO_2$ catalyst for CO oxidation, Catal. Today 280 (2017) 239–245.
[11] G. Ma, A. Binder, M. Chi, C. Liu, R. Jin, D. Jiang, J. Fan, S. Dai, Stabilizing gold clusters by heterostructured transition-metal oxide–mesoporous silica supports for enhanced catalytic activities for CO oxidation, Chem. Commun. 48 (2012) 11413–11415.
[12] X. Nie, H. Qian, Q. Ge, H. Xu, R. Jin, CO Oxidation Catalyzed by Oxide-Supported $Au_{25}(SR)_{18}$ Nanoclusters and Identification of Perimeter Sites as Active Centers, ACS Nano 6 (2012) 6014–6022.
[13] X. Nie, C. Zeng, X. Ma, H. Qian, Q. Ge, H. Xu, R. Jin, CeO2-supported $Au_{38}(SR)_{24}$ nanocluster catalysts for CO oxidation: a comparison of ligand-on and -off catalysts, Nanoscale 5 (2013) 5912–5918.
[14] Z. Wu, D. Jiang, A.K.P. Mann, D.R. Mullins, Z.A. Qiao, L.F. Allard, C. Zeng, R. Jin, S.H. Overbury, Thiolate Ligands as a Double-Edged Sword for CO Oxidation on CeO_2 Supported $Au_{25}(SCH_2CH_2Ph)_{18}$ Nanoclusters, J. Am. Chem. Soc. 136 (2014) 6111–6122.
[15] K. Zheng, M.I. Setyawati, T.P. Lim, D.T. Leong, J. Xie, Antimicrobial Cluster Bombs: Silver Nanoclusters Packed with Daptomycin, ACS Nano 10 (2016) 7934–7942.
[16] O. Lopez-Acevedo, K.A. Kacprzak, J. Akola, H. Häkkinen, Quantum size effects in ambient CO oxidation catalysed by ligand-protected gold clusters, Nat. Chem. 2 (2010) 329–334.
[17] X. Kong, H. Zhu, C. Chen, G. Huang, Q. Chen, Insights into the reduction of 4-nitrophenol to 4-aminophenol on catalysts, Chem. Phys. Lett. 684 (2017) 148–152.
[18] Z. Li, C. Liu, H. Abroshan, D.R. Kauffman, G. Li, $Au_{38}S_2(SAdm)_{20}$ Photocatalyst for One-Step Selective Aerobic Oxidations, ACS Catal. 7 (2017) 3368–3374.
[19] G. Li, H. Qian, R. Jin, Gold nanocluster-catalyzed selective oxidation of sulfide to sulfoxide, Nanoscale 4 (2012) 6714–6717.
[20] J. Liu, K.S. Krishna, Y.B. Losovyj, S. Chattopadhyay, N. Lozova, J.T. Miller, J. J. Spivey, C.S.S.R. Kumar, Ligand-Stabilized and Atomically Precise Gold Nanocluster Catalysis: A Case Study for Correlating Fundamental Electronic Properties with Catalysis, Chem. Eur. J. 19 (2013) 10201–10208.
[21] Y. Liu, H. Tsunoyama, T. Akita, T. Tsukuda, Efficient and selective epoxidation of styrene with TBHP catalyzed by Au_{25} clusters on hydroxyapatite, Chem. Commun. 46 (2010) 550–552.

[22] S. Zhao, A. Das, H. Zhang, R. Jin, Y. Song, R. Jin, Mechanistic insights from atomically precise gold nanocluster-catalyzed reduction of 4-nitrophenol, Prog. Nat. Sci. 26 (2016) 483–486.

[23] M. Dasog, W. Hou, R.W.J. Scott, Controlled growth and catalytic activity of gold monolayer protected clusters in presence of borohydride salts, Chem. Commun. 47 (2011) 8569–8571.

[24] H. Chong, P. Li, J. Xiang, F. Fu, D. Zhang, X. Ran, M. Zhu, Design of an ultrasmall Au nanocluster–CeO_2 mesoporous nanocomposite catalyst for nitrobenzene reduction, Nanoscale 5 (2013) 7622–7628.

[25] H. Chong, P. Li, S. Wang, F. Fu, J. Xiang, M. Zhu, Y. Li, Au_{25} Clusters as Electron-Transfer Catalysts Induced the Intramolecular Cascade Reaction of 2-nitrobenzonitrile, Sci. Rep. 3 (2013) 3214.

[26] Y. Zhu, Z. Wu, C. Gayathri, H. Qian, R.R. Gil, R. Jin, Exploring stereoselectivity of Au_{25} nanoparticle catalyst for hydrogenation of cyclic ketone, J. Catal. 271 (2010) 155–160.

[27] G. Li, R. Jin, Gold Nanocluster-Catalyzed Semihydrogenation: A Unique Activation Pathway for Terminal Alkynes, J. Am. Chem. Soc. 136 (2014) 11347–11354.

[28] G. Li, C. Zeng, R. Jin, Thermally robust $Au_{99}(SPh)_{42}$ nanoclusters for chemoselective hydrogenation of nitrobenzaldehyde derivatives in water, J. Am. Chem. Soc. 136 (2014) 3673–3679.

[29] G. Li, D. Jiang, S. Kumar, Y. Chen, R. Jin, Size Dependence of Atomically Precise Gold Nanoclusters in Chemoselective Hydrogenation and Active Site Structure, ACS Catal. 4 (2014) 2463–2469.

[30] G. Li, H. Abroshan, Y. Chen, R. Jin, H.J. Kim, Experimental and Mechanistic Understanding of Aldehyde Hydrogenation Using Au_{25} Nanoclusters with Lewis Acids: Unique Sites for Catalytic Reactions, J. Am. Chem. Soc. 137 (2015) 14295–14304.

[31] Y. Zhu, H. Qian, B.A. Drake, R. Jin, Atomically precise $Au_{25}(SR)_{18}$ nanoparticles as catalysts for the selective hydrogenation of alpha,beta-unsaturated ketones and aldehydes, Angew. Chem. Int. Ed. 49 (2010) 1295–1298.

[32] G. Li, C. Liu, Y. Lei, R. Jin, Au_{25} nanocluster-catalyzed Ullmann-type homocoupling reaction of aryl iodides, Chem. Commun. 48 (2012) 12005–12007.

[33] G. Li, H. Abroshan, C. Liu, S. Zhuo, Z. Li, Y. Xie, H.J. Kim, N.L. Rosi, R. Jin, Tailoring the Electronic and Catalytic Properties of Au_{25} Nanoclusters via Ligand Engineering, ACS Nano 10 (2016) 7998–8005.

[34] G. Li, D. Jiang, C. Liu, C. Yu, R. Jin, Oxide-supported atomically precise gold nanocluster for catalyzing Sonogashira cross-coupling, J. Catal. 306 (2013) 177–183.

[35] H. Abroshan, G. Li, J. Lin, H.J. Kim, R. Jin, Molecular mechanism for the activation of $Au_{25}(SCH_2CH_2Ph)_{18}$ nanoclusters by imidazolium-based ionic liquids for catalysis, J. Catal. 337 (2016) 72–79.

[36] S. Zhao, R. Jin, H. Abroshan, C. Zeng, H. Zhang, S.D. House, E. Gottlieb, H.J. Kim, J.C. Yang, R. Jin, Gold Nanoclusters Promote Electrocatalytic Water Oxidation at the Nanocluster/$CoSe_2$ Interface, J. Am. Chem. Soc. 139 (2017) 1077–1080.

[37] Q. Wang, L. Wang, Z. Tang, F. Wang, W. Yan, H. Yang, W. Zhou, L. Li, X. Kang, S. Chen, Oxygen reduction catalyzed by gold nanoclusters supported on carbon nanosheets, Nanoscale 8 (2016) 6629–6635.

[38] D.R. Kauffman, D. Alfonso, C. Matranga, H. Qian, R. Jin, Experimental and Computational Investigation of Au_{25} Clusters and CO_2 : A Unique Interaction and Enhanced Electrocatalytic Activity, J. Am. Chem. Soc. 134 (2012) 10237–10243.

[39] J. Li, R.R. Nasaruddin, Y. Feng, J. Yang, N. Yan, J. Xie, Tuning the Accessibility and Activity of $Au_{25}(SR)_{18}$ Nanocluster Catalysts through Ligand Engineering, Chem. Eur. J. 22 (2016) 14816–14820.

[40] Z. Li, X. Yang, C. Liu, J. Wang, G. Li, Effects of doping in 25-atom bimetallic nanocluster catalysts for carbon-carbon coupling reaction of iodoanisole and phenylacetylene, Prog. Nat. Sci. Mater. Int. 26 (2016) 477–482.

[41] H. Chen, C. Liu, M. Wang, C. Zhang, N. Luo, Y. Wang, H. Abroshan, G. Li, F. Wang, Visible Light Gold Nanocluster Photocatalyst: Selective Aerobic Oxidation of Amines to Imines, ACS Catal. 7 (2017) 3632–3638.

[42] X. Dou, X. Yuan, Q. Yao, Z. Luo, K. Zheng, J. Xie, Facile synthesis of water-soluble $Au_{25-X}Ag_X$ nanoclusters protected by mono- and bi-thiolate ligands, Chem. Commun. 50 (2014) 7459–7462.

[43] A.L. Gould, C.J. Heard, A.J. Logsdail, C.R.A. Catlowac, Segregation effects on the properties of $(AuAg)_{147}$, Phys. Chem. Chem. Phys. 16 (2014) 21049–21061.

[44] H. Yao, R. Kobayashi, Y. Nonoguch, Enhanced Chiroptical Activity in Glutathione-Protected Bimetallic $(AuAg)_{18}$ Nanoclusters with Almost Intact Core−Shell Configuration, J. Phys. Chem. C 120 (2016) 1284–1292.

[45] R.D. Corpuz, Y. Ishida, M.T. Nguyen, T. Yonezawa, Synthesis of Positively Charged Photoluminescent Bimetallic Au-Ag Nanoclusters by Double-Target Sputtering Method on a Biocompatible Polymer Matrix, Langmuir 33 (2017) 9144–9150.

[46] Y. Wang, H. Su, C. Xu, G. Li, L. Gell, S. Lin, Z. Tang, H. Häkkinen, N. Zheng, An Intermetallic $Au_{24}Ag_{20}$ Superatom Nanocluster Stabilized by Labile Ligands, J. Am. Chem. Soc. 137 (2015) 4324–4327.

[47] Z. Wang, R. Senanayake, C.M. Aikens, W.M. Chen, C.H. Tunga, D. Sun, Gold-doped silver nanocluster $[Au_3Ag_{38}(SCH_2Ph)_{24}X_5]^{2-}$ (X = Cl or Br), Nanoscale 8 (2016) 18905–18911.

[48] S. Jin, W. Du, S. Wang, X. Kang, M. Chen, D. Hu, S. Chen, X. Zou, G. Sun, M. Zhu, Thiol-Induced Synthesis of Phosphine-Protected Gold Nanoclusters with Atomic Precision and Controlling the Structure by Ligand/Metal Engineering, Inorg. Chem. 56 (2017) 11151–11159.

[49] Q.M. Deng, L.X. Zhao, X.J. Feng, M. Zhang, W.L. Zhang, B. Fang, Y.H. Luo, Exploring stability of 32-atom gold–silver mixed clusters, Comput. Theor. Chem. 976 (2011) 183–187.

[50] X. Dou, X. Yuan, Y. Yu, Z. Luo, Q. Yao, D.T. Leong, J. Xie, Lighting up thiolated Au@Ag nanoclusters via aggregation-induced emission, Nanoscale 6 (2014) 157–161.

[51] Y. Wang, X.K. Wan, L. Ren, H. Su, G. Li, S. Malola, S. Lin, Z. Tang, H. Häkkinen, B. K. Teo, Q.M. Wang, N. Zheng, Atomically Precise Alkynyl-Protected Metal Nanoclusters as a Model Catalyst: Observation of Promoting Effect of Surface Ligands on Catalysis by Metal Nanoparticles, J. Am. Chem. Soc. 138 (2016) 3278–3281.

[52] G. Soldan, M.A. Aljuhani, M.S. Bootharaju, L.G. Abdul Halim, M.R. Parida, A. H. Emwas, O.F. Mohammed, O.M. Bakr, Gold Doping of Silver Nanoclusters: A 26-Fold Enhancement in the Luminescence Quantum Yield, Angew. Chem. Int. Ed. 55 (2016) 5749–5753.

[53] S. Wang, H. Abroshan, C. Liu, T.Y. Luo, M. Zhu, H.J. Kim, N.L. Rosi, R. Jin, Shuttling single metal atom into and out of a metal nanoparticle, Nat. Commun. 8 (2017) 848.

[54] K.R. Krishnadas, A. Ghosh, A. Baksi, I. Chakraborty, G. Natarajan, T. Pradeep, ntercluster Reactions between $Au_{25}(SR)_{18}$ and $Ag_{44}(SR)_{30}$, J. Am. Chem. Soc. 138 (2016) 140–148.

[55] K.R. Krishnadas, A. Baksi, A. Ghosh, G. Natarajan, T. Pradeep, Structure-conserving spontaneous transformations between nanoparticles, Nat. Commun. 7 (2016) 13447.

[56] J.L. Zeng, Z.J. Guan, Y. Du, Z.A. Nan, Y.M. Lin, Q.M. Wang, Chloride-Promoted Formation of a Bimetallic Nanocluster $Au_{80}Ag_{30}$ and the Total Structure Determination, J. Am. Chem. Soc. 138 (2021) 7848–7851.

[57] Z. Lei, X.L. Pei, Z.J. Guan, Q.M. Wang, Full Protection of Intensely Luminescent Gold(I)-Silver(I) Cluster by Phosphine Ligands and Inorganic Anions, Angew. Chem. Int. Ed. 56 (2017) 7117–7120.

[58] C. Yao, J. Chen, M.B. Li, L. Liu, J. Yang, Z. Wu, Adding two active silver atoms on Au_{25} nanoparticle, Nano Lett. 15 (2015) 1281–1287.

[59] Z. Wu, Anti-Galvanic Reduction of Thiolate-Protected Gold and Silver Nanoparticles, Angew. Chem. Int. Ed. 51 (2012) 2934–2938.

[60] H. Yang, Y. Wang, H. Huang, L. Gell, L. Lehtovaara, S. Malola, H. Häkkinen, N. Zheng, All-thiol-stabilized Ag_{44} and $Au_{12}Ag_{32}$ nanoparticles with single-crystal structures, Nat. Commun. 4 (2013) 2422.

[61] Y. Zhou, H.C. Zeng, Transition-Metal-Ions-Induced Coalescence: Stitching Au Nanoclusters into Tubular Au-Based Nanocomposites, Small 12 (2016) 2652–2664.

[62] S. Wang, Y. Song, S. Jin, X. Liu, J. Zhang, Y. Pei, X. Meng, M. Chen, P. Li, M. Zhu, Metal Exchange Method Using Au_{25} Nanoclusters as Templates for Alloy Nanoclusters with Atomic Precision, J. Am. Chem. Soc. 137 (2015) 4018–4021.

[63] X. Kang, S. Wang, Y. Song, S. Jin, G. Sun, H. Yu, M. Zhu, Bimetallic Au_2Cu_6 Nanoclusters: Strong Luminescence Induced by the Aggregation of Copper(I) Complexes with Gold(0) Species, Angew. Chem. Int. Ed. 55 (2016) 3611–3614.

[64] L.E. Marbella, D.M. Chevrier, P.D. Tancini, O. Shobayo, A.M. Smith, K.A. Johnston, C.M. Andolina, P. Zhang, G. Mpourmpakis, J.E. Millstone, Description and Role of Bimetallic Prenucleation Species in the Formation of Small Nanoparticle Alloys, J. Am. Chem. Soc. 137 (2015) 15852–15858.

[65] X.K. Wan, X.L. Cheng, Q. Tang, Y.Z. Han, G. Hu, D.E. Jiang, Q.M. Wang, Atomically Precise Bimetallic $Au_{19}Cu_{30}$ Nanocluster with an Icosidodecahedral Cu_{30} Shell and an Alkynyl-Cu Interface, J. Am. Chem. Soc. 139 (2017) 9451–9454.

[66] H. Yang, Y. Wang, J. Lei, L. Shi, X. Wu, V. M, S. Lin, Z. Tang, J. He, H. Häkkinen, L. Zheng, N. Zheng, Ligand-stabilized $Au_{13}Cu_x$ (x = 2, 4, 8) bimetallic nanoclusters: ligand engineering to control the exposure of metal sites, J. Am. Chem. Soc. 135 (2013) 9568–9571.

[67] H. Yang, Y. Wang, J. Yan, X. Chen, X. Zhang, H. Häkkinen, N. Zheng, Structural Evolution of Atomically Precise Thiolated Bimetallic $[Au_{12+n}Cu_{32}(SR)_{30+n}]^{4-}$ (n = 0, 2, 4, 6) Nanoclusters, J. Am. Chem. Soc. 136 (2014) 7197–7200.

[68] K. Kwak, Q. Tang, M. Kim, D. Jiang, D. Lee, Interconversion between Superatomic 6-Electron and 8-Electron Configurations of $M@Au_{24}(SR)_{18}$ Clusters (M = Pd, Pt), J. Am. Chem. Soc. 137 (2015) 10833–10840.

[69] H. Qian, D.E. Jiang, G. Li, C. Gayathri, A. Das, R.R. Gil, R. Jin, Monoplatinum Doping of Gold Nanoclusters and Catalytic Application, J. Am. Chem. Soc. 134 (2012) 16159–16162.

[70] K. Kwak, W. Choi, Q. Tang, M. Kim, Y. Lee, D. Jiang, D. Lee, A molecule-like $PtAu_{24}(SC_6H_{13})_{18}$ nanocluster as an electrocatalyst for hydrogen production, Nat. Commun. 8 (2016) 14723.

[71] M. Zhou, Y.Q. Cai, M.G. Zeng, C. Zhang, Y.P. Feng, Mn-doped thiolated Au_{25} nanoclusters: Atomic configuration, magnetic properties, and a possible high-performance spin filter, Appl. Phys. Lett. 98 (2011), 143103.

[72] X. Wei, R. Zhou, W. Lefebvre, K. He, D.L. Roy, R. Skomski, X. Li, J.E. Shield, M. J. Kramer, S. Chen, X.C. Zeng, D.J. Sellmyer, Structural and Magnetic Evolution of Bimetallic MnAu Clusters Driven by Asymmetric Atomic Migration, Nano Lett. 14 (2014) 1362.

[73] L. Liao, S. Zhou, Y. Dai, L. Liu, C. Yao, C. Fu, J. Yang, Z. Wu, Mono-Mercury Doping of Au_{25} and the HOMO/LUMO Energies Evaluation Employing Differential Pulse Voltammetry, J. Am. Chem. Soc. 137 (2015) 9511–9514.

[74] C. Yao, Y.J. Lin, J. Yuan, L. Liao, M. Zhu, L.H. Weng, J. Yang, Z. Wu, Mono-cadmium vs Mono-mercury Doping of Au_{25} Nanoclusters, J. Am. Chem. Soc. 137 (2015) 15350–15353.

[75] H. Deng, S. Wang, S. Jin, S. Yang, Y. Xu, L. Liu, J. Xiang, D. Hu, M. Zhu, Active metal (cadmium) doping enhanced the stability of inert metal (gold) nanocluster under O_2 atmosphere and the catalysis activity of benzyl alcohol oxidation, Gold Bull. 48 (2015) 161–167.

[76] M.B. Li, S.K. Tian, Z. Wu, Improving the Catalytic Activity of Au_{25} Nanocluster by Peeling and Doping, Chin. J. Chem. 35 (2017) 567–571.

[77] D. Bhattacharjee, B.K. Mishra, R.C. Deka, Effect of double aluminium doping on the structure, stability and electronic properties of small gold clusters, J. Mater. Sci. 50 (2015) 4586–4599.

[78] Q. Yao, Y. Feng, V. Fung, Y. Yu, D.E. Jiang, J. Yang, J. Xie, Precise control of alloying sites of bimetallic nanoclusters via surface motif exchange reaction, Nat. Commun. 8 (2017) 1555.
[79] G. Li, R. Jin, Atomic level tuning of the catalytic properties: Doping effects of 25-atom bimetallic nanoclusters on styrene oxidation, Catal. Today 278 (2016) 187–191.
[80] A.V. Marenich, S.V. Jerome, C.J. Cramer, D.G. Truhlar, An Extension of Hirshfeld Population Analysis for the Accurate Description of Molecular Interactions in Gaseous and Condensed Phases, J. Chem. Theory Comput. 8 (2012) 527–541.
[81] J. Akola, M. Walter, R.L. Whetten, H. Häkkinen, H. Grönbeck, On the structure of thiolate-protected Au_{25}, J. Am. Chem. Soc. 130 (2008) 3756–3757.
[82] C. Liu, S. Lin, Y. Pei, X.C. Zeng, Semiring Chemistry of $Au_{25}(SR)_{18}$: Fragmentation Pathway and Catalytic Active site, J. Am. Chem. Soc. 135 (2013) 18067–18079.
[83] J. Cai, H. Ma, J. Zhang, Q. Song, Z. Du, Y. Huang, J. Xu, Gold Nanoclusters Confined in a Supercage of Y Zeolite for Aerobic Oxidation of HMF under Mild Conditions, Chem. Eur. J. 19 (2013) 14215–14223.
[84] S. Matsuo, S. Yamazoe, J.Q. Goh, J. Akolacd, T. Tsukuda, The electrooxidation-induced structural changes of gold di-superatomic molecules: Au_{23} vs. Au_{25}, Phys. Chem. Chem. Phys. 18 (2015) 4822–4827.
[85] R. Jin, Atomically precise metal nanoclusters: stable sizes and optical properties, Nanoscale 7 (2015) 1549–1565.
[86] H. Yamamoto, H. Yano, H. Kouchi, Y. Obora, R. Arakawa, H. Kawasaki, N,N-Dimethylformamide-stabilized gold nanoclusters as a catalyst for the reduction of 4-nitrophenol, Nanoscale 4 (2012) 4148–4154.
[87] R.R. Nasaruddin, Q. Yao, T. Chen, M.J. Hülsey, N. Yan, J. Xie, Hydride-induced ligand dynamic and structural transformation of gold nanoclusters during a catalytic reaction, Nanoscale 10 (2018) 23113–23121.
[88] M.A. Koklioti, T. Skaltsas, Y. Sato, K. Suenaga, A. Stergiou, N. Tagmatarchis, Mechanistic insights into the photocatalytic properties of metal nanocluster/graphene ensembles. Examining the role of visible light in the reduction of 4-nitrophenol, Nanoscale 9 (2017) 9685–9692.
[89] A.H. Pakiari, Z. Jamshidi, Nature and Strength of M-S Bonds (M) Au, Ag, and Cu) in Binary Alloy Gold Clusters, J. Phys. Chem. A 114 (2010) 9212–9221.
[90] Y. Chen, C. Liu, H. Abroshan, Z. Li, J. Wang, G. Li, M. Haruta, Phosphine/phenylacetylide-ligated Au clusters for multicomponent coupling reactions, J. Catal. 340 (2016) 287–294.
[91] Z. Li, W. Li, H. Abroshan, Q. Ge, G. Li, R. Jin, Dual effects of water vapor on ceria-supported gold clusters, Nanoscale 10 (2018) 6558–6565.
[92] W. Li, C. Liu, H. Abroshan, Q. Ge, X. Yang, H. Xu, G. Li, Catalytic CO Oxidation Using Bimetallic M_xAu_{25-x} Clusters: A Combined Experimental and Computational Study on Doping Effects, J. Phys. Chem. C 120 (2016) 10261–10267.
[93] Z.Y. Li, J.P. Wilcoxon, F. Yin, Y. Chen, R.E. Palmer, R.L. Johnston, Structures and optical properties of 4–5 nm bimetallic AgAu nanoparticles, Faraday Discuss. 138 (2008) 363–373.
[94] L. Chen, C.P. Deming, Y. Peng, P. Hu, J. Stofan, S. Chen, Gold core@silver semishell Janus nanoparticles prepared by interfacial etching, Nanoscale 8 (2016) 14565–14572.
[95] M.S. Bootharaju, R. Dey, L.E. Gevers, M.N. Hedhili, J.M. Basset, O.M. Bakr, A New Class of Atomically Precise, Hydride-Rich Silver Nanoclusters Co-Protected by Phosphines, J. Am. Chem. Soc. 138 (2016) 13770–13773.
[96] P. Pyykkö, Theoretical Chemistry of Gold, Angew. Chem. Int. Ed. 43 (2004) 4412–4456.
[97] S. Back, M.S. Yeom, Y. Jung, Active Sites of Au and Ag Nanoparticle Catalysts for CO_2 Electroreduction to CO, ACS Catal. 5 (2015) 5089–5096.